J. Fluid Mech. (1972), *vol.* 53, *part* 3, *pp.* 481–512
Printed in Great Britain

On the movement of water and solute in extracellular channels with filtration, osmosis and active transport

By SHELDON WEINBAUM
City College, City University of New York
AND J. RICHARD GOLDGRABEN
Polytechnic Institute of Brooklyn

(Received 27 September 1971)

A quantitative two-dimensional theoretical model is developed to describe the movement of water and salt along the long narrow extracellular channels which appear to be a common structural feature of all epithelial membranes. This study examines the transport behaviour of both open and closed membrane systems as a function of the geometric specialization of the channel and the active transport site location under the influence of three driving forces: transmembrane osmotic and hydrodynamic pressure differentials and active transport. The previous one-dimensional hydrodynamic model of Diamond & Bossert (1967) and Segel (1970) was confined to closed channel systems such as the gall bladder in which the only mechanism for water movement is local osmosis due to active transport.

Approximate analytical solutions are presented for long constant-area open channels in which the active transport sites have been idealized as point solute sources. A streamwise co-ordinate straining technique has been used in these solutions to describe the nonlinear effects of convection over long distances. Closed-form solutions are also presented for the pressure and solute concentration distributions within simplified models of channel constrictions with varying degrees of occlusion.

Numerical results of the model have been compared with Cole's (1961, 1962) *in vivo* and *in vitro* experiments on the rabbit ciliary body. Satisfying agreement with the measured values of the solute and water fluxes has been obtained for both the living eye and the excised ciliary body. These results strongly suggest that the formation of aqueous humour in the rabbit is a pressure-dependent process in which local osmosis due to active transport accounts for only one-third of the total aqueous flow. The model has also been applied to the gall bladder epithelium using more general boundary conditions than allowed for in the model of Diamond & Bossert. New solutions yielding a vanishing diffusional flux at the channel exit were obtained. However, the model, like that of Diamond & Bossert, does not provide a rational explanation as to how the water in the cell interior is replenished.

1. Background physiology

Epithelial membranes have long been of interest to physiologists and the medical profession because of their widespread occurrence in human and animal organs and because of their intriguing ability to transport water and solute between bathing solutions which are either isotonic or have hydrostatic and electrochemical gradients counter to the direction of flow. Such cell layers are present in the ciliary processes of the eye, the gall bladder, the renal proximal tubule, the intracellular canaliculi of the small intestine, the avian salt gland, frog skin and numerous other animal and human organs. The primary emphasis of the present paper is the development of a mathematical model for porous epithelia with pressure filtration and active transport, and its application, in particular, to the ciliary body epithelium. Model predictions for the water and solute fluxes are in good quantitative agreement with Cole's (1961, 1962) detailed measurements of the transport of aqueous humour in both living cat and rabbit eyes and in the excised ciliary body. For tight juncture or non-porous epithelia Diamond & Bossert (1967, hereafter referred to as DB) have formulated an ingenious mathematical model to describe the standing-gradient osmotic flow established when there is no filtration. This model has provided valuable insight in explaining Diamond's (1964) measurements of isotonic transport in the gall bladder. The present model has also been applied to the gall bladder using more general boundary and initial conditions for the extracellular channels than previously considered in DB. A new family of solutions permitting a vanishing concentration gradient at the channel exit was discovered but the results, like those reported in DB, do not offer a satisfactory explanation as to how the water in the cell interior is replenished.

Figure 1 is a schematic diagram taken from Diamond & Tormey (1966) and shows what one would observe in an electron micrograph of the gall bladder epithelium. This membrane is a simple monolayer. The movement of water and salt across the membrane from the lumen or gall bladder sac is assumed to occur via tortuous extracellular channels which are closed at the lumenal end by junctional complexes, or terminal bars. These complexes are assumed to form a solute and watertight seal. The energy for the water and solute movement is derived from metabolically linked ion pumps or secretory sites that histochemical studies show to be located along the intercellular membranes that form the boundaries of the extracellular channels. In the gall bladder the active transport of chloride ions is accompanied by an equal movement of sodium ions to maintain electroneutrality. In other epithelial cell layers the movement of the anion or cation may be partially or totally inhibited. The pump then acts as a battery which produces charge separation and a potential difference across the membrane.

The conceptual basis for the standing-gradient osmotic model is that sodium and chloride ions are actively pumped into the extracellular channels near their closed end from secretory sites located on the intercellular membranes. The local osmotic gradient established by this pumping action draws water passively from the cell interior into the channel. To conserve mass, both water and solute are forced out of the open end of the channel because of the build up of pressure at the

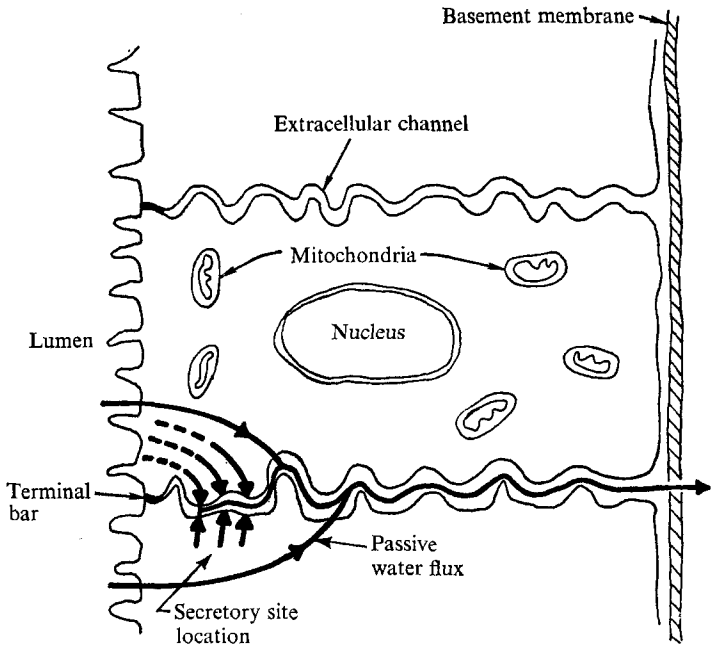

FIGURE 1. Schematic diagram of gall bladder epithelial membrane (based on Diamond & Tormey 1966).

closed end. For steady-state operation both the water and salt are replenished from the inner bathing solution in the lumen. The effluent at the channel exit can by hypertonic, isotonic or hypotonic with respect to the lumenal fluid. The intriguing feature of gall bladder transport is that, over a wide concentration range, the exuded fluid is isotonic with the salt solution in the lumen and that transport occurs in the absence of a transmembrane pressure differential, see Diamond (1964). Other membranes, such as the avian salt gland, teleost intestine and the ciliary processes transport a slightly hypertonic fluid.

The mathematical model developed in DB to describe the above behaviour treats the extracellular channel as a one-dimensional flow in a constant-area cylindrical pore of circular cross-section. Both the solute and total mass are conserved in the channel interior, while the lateral boundary conditions allow for active transport of salt and passive movement of water, but not salt, across the intercellular membranes. Both the water and solute fluxes at the closed end (initial station) are zero while the concentration C_{s0} in the cell interior is assumed well mixed and hence uniform. The boundary-value problem just described is not unique since the initial concentration $C_s(0)$ can take on any value. In DB, $C_s(0)$ is uniquely determined for a channel of given length L by requiring that the dimensionless exit concentration $C_s(L) = 1$, that is, that the channel effluent should be isotonic with the solution in the cell interior. This is one of the weaknesses of the DB model since in reality $C_s(L)$ can have any value. It is neither the concentration of a well stirred outer bathing solution (a concentration boundary layer could exist) or the concentration that would be measured if the effluent was allowed to drip off the gall bladder sac and be collected in a beaker. The

latter concentration is given by $Q_s(L)/Q(L)$, where $Q_s(L)$ and $Q(L)$ are the total solute and water fluxes at the channel exit; $Q_s(L)$ includes both a convective and a diffusional component unless $dC_s(L)/dx = 0$. Therefore, in specifying $C_s(L)$ the channel flow behaviour is constrained unnecessarily. For this reason no exit boundary condition is prescribed in the present study but rather $C_s(0)$ is varied as a free parameter, each assumed initial concentration yielding a different solution. We shall observe later that this extra degree of freedom leads to a new family of solutions that is not contained in the DB analysis.

The fundamental question that is not answered by the standing-gradient osmotic model at present is how the water in the cell interior is replenished. It would seem reasonable to expect this water to be derived from the lumenal fluid, the transport occurring through a local osmotic gradient at the inner membrane. This requirement is not satisfied by the DB model since the osmolarity of the lumenal fluid and that in the cell interior are assumed equal. For self consistency the condition of isotonic transport in Diamond's (1964) experiments would appear to require that the concentration of the lumenal fluid be hypotonic relative to the solution in the cell interior and isotonic with respect to both the channel effluent and the outer bathing solution. The latter requires that a concentration boundary layer should not exist at the channel exit and hence that $dC_s(L)/dx = 0$. Thus, in contrast to Diamond & Bossert, we ask whether it is possible for a finite-length channel to have an effluent which is hypotonic relative to the cell interior solution and at the same time have a vanishing gradient at the exit plane. Approximate analytic solutions to the equations and boundary conditions in DB based on a small parameter expansion have been presented by Segel (1970). The governing equations are non-dimensionalized in a manner similar to that presented here and the basic dimensionless groupings that characterize the DB model are derived. These solutions compare well with numerical results of DB over most of the anticipated range of values for the membrane parameters.

In contrast to the relatively simple gall bladder monolayer depicted in figure 1, figure 2 shows schematically what one would observe in an electron micrograph of the considerably more complex epithelium in the ciliary processes of the eye. This membrane secretes a slightly hypertonic salt solution called aqueous humour into the posterior chamber behind the lens at a relatively high rate which ranges from 0·4 to 3 μl min^{-1} cm^{-2} for human and cat's eyes respectively. The membrane is a dual cell layer comprising pigmented and non-pigmented cells. While the details in the ultrastucture of the membrane are not as well documented as for the gall bladder, there is a significant body of evidence suggesting that the extracellular channels provide a direct link between the inner (stromal) and outer (posterior chamber) fluids, but contain partially occluded zones whose physiological function is not understood. The apical infoldings shown in the sketch are actually interface projections of adjacent cells above and below the plane of the micrograph. Histochemical studies of ATPase activity show that active transport sites are located largely in the lateral infoldings of the non-pigmented cell layer. Thus, the position of the secretory sites relative to the channel exit is just the opposite of that in the gall bladder.

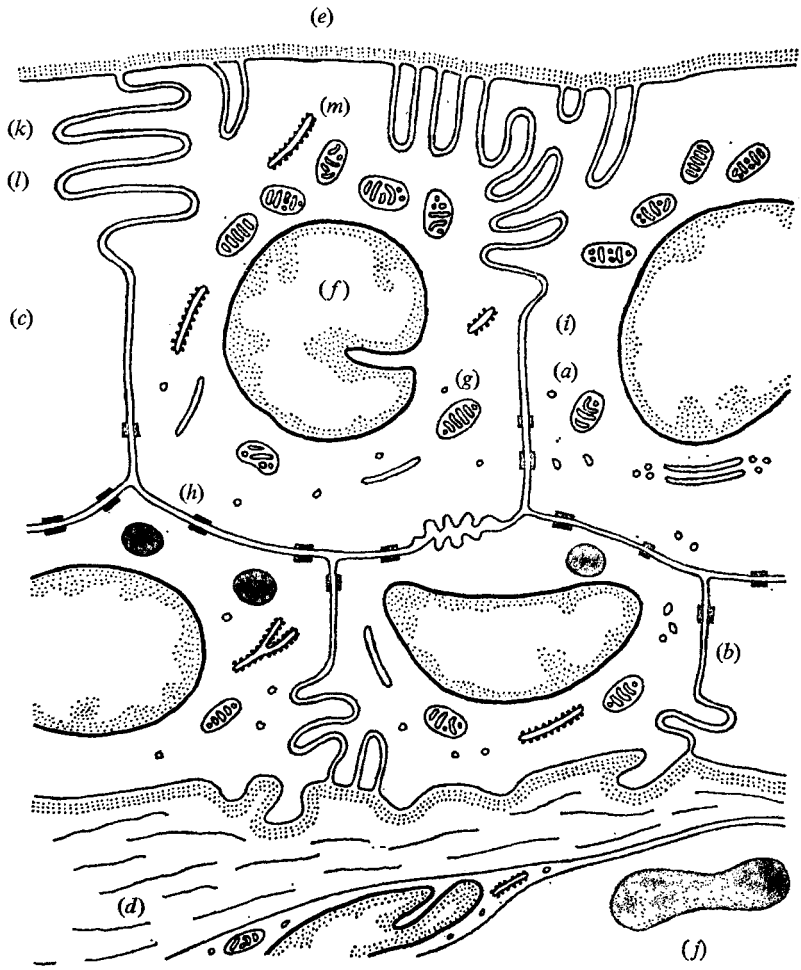

FIGURE 2. Schematic diagram of ciliary body epithelial membrane showing: (*a*) extracellular channels, (*b*) pigmented layer, (*c*) non-pigmented layer, (*d*) stromal fluid, (*e*) posterior chamber fluid, (*f*) cell nuclei, (*g*) mitochondria, (*h*) desmosomes, (*i*) partially occluded zones, (*j*) red blood cell, (*k*) proposed secretory site based on ATPase activity, (*l*) lateral infoldings, (*m*) apical infoldings.

In the absence of junctional complexes both water and solute will have finite fluxes at the channel entrance. Excluding electrical effects, two additional driving forces for the channel flow must be considered; these were not present in the standing-gradient osmotic model for the gall bladder. Thus, three driving forces of non-electrical origin can be anticipated to contribute to the total water and solute movement in porous epithelia with secretory sites: active transport due to the ion pump (local osmosis), concentration difference between inner and outer bathing solutions (osmosis), and filtration due to the hydrodynamic pressure difference between the interstitial pressure in the stromal fluid and the intraocular pressure in the posterior chamber.

One important and heretofore unexplained feature of ciliary body transport

which the present model will attempt to answer is the large and disproportionate difference in the measured water and solute fluxes in living and excised eyes of both the cat and rabbit. In the experiments of Cole (1961, 1962), for example, the measured aqueous flux *in vivo* was five times greater than that in excised preparations, while the sodium flux *in vivo* was only 50% greater than that in the preparation. In addition, active transport accounted for all of the sodium flux in the excised preparation while accounting for only 30% *in vivo*.

The mathematical model for the extracellular channel developed by the authors contains two fundamental generalizations of the basic DB model. One is the introduction of a new equation, a momentum conservation equation for bulk fluid movement; the second is the treatment of the boundary conditions at the channel entrance and exit. The initial conditions for both the bulk velocity and concentration gradient are both unknown in contrast to the DB standing-gradient model, where they are assumed to be zero. In their place the two new driving forces, pressure filtration and osmosis, require more difficult split boundary conditions for the transmembrane pressure and concentration difference respectively. The present model also contains three refinements of interest: the use of a two-dimensional velocity profile description, instead of the uniform slug profile of DB, to describe the shearing stress due to the velocity gradient at the lateral boundaries; the treatment of variable-area channels including analytic solutions for some simple constriction geometries; and the introduction of two-dimensional concentration profiles so that the instantaneous mixing hypothesis can be relaxed for channels where L/h is not $\gg 1$.

Section 2 presents the formulation of the pertinent conservation relations for the channel flow. Section 3 describes some approximate analytic solutions for constant-area open channels with combined active transport and filtration. The numerical solutions are presented in §§ 4 and 5 for closed and open channels respectively. Section 6 gives a simplified analytical treatment of the effect of partially occluded regions.

2. Mathematical model

In this section we shall formulate the mathematical boundary-value problem that describes the transport phenomena occurring in the mathematical model of the generalized electroneutral extracellular channel shown schematically in figure 3. We wish to determine the various velocity, solute concentration and pressure fields that can emerge when varied boundary conditions are applied at the channel ends and along the intercellular membranes which form the lateral walls of the channel. The fluid in the channel is assumed to be a two-species continuum of solute and solvent and to have two-dimensional field properties. The desired field descriptions could be obtained from the well-known partial differential equations for overall continuity, conservation of solute and the Navier–Stokes momentum equation. The use of such a system of exact equations involves, however, a degree of mathematical complexity which in light of the present status of our understanding of the relevant physiological phenomena on a molecular level does not seem justified. Accordingly, we shall develop instead

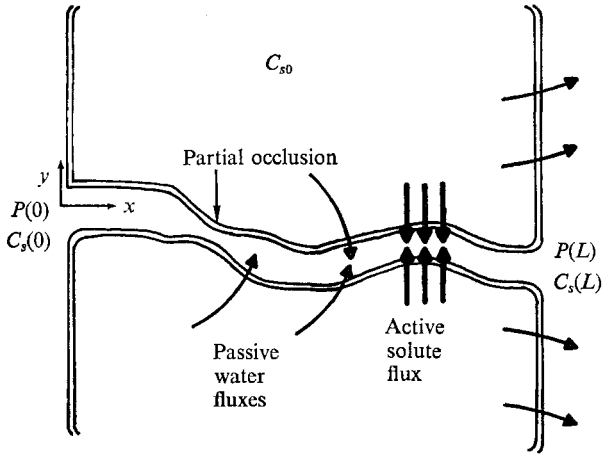

FIGURE 3. Generalized extracellular channel model.

a simplified description using integral techniques that will enable us to reduce the conservation relations for the channel to a system of ordinary differential equations satisfying appropriate boundary conditions. This approach permits us to retain an approximate two-dimensional description of the velocity and solute concentration fields, and, therefore, allows us to study the shear-stress distribution and the mixing normal to the lateral boundaries of the channel.

For the aforementioned purposes the channel is divided into a series of infinitesimal control volume elements of length Δx, unit depth and height h, which is assumed to be a slowly varying function of the streamwise co-ordinate x. An active solute flux and a passive water flux are assumed to enter the volume element symmetrically across the lateral boundaries.

2.1. *Overall continuity equation*

Conservation of total mass within the differential control volume of length Δx requires that the net mass flux of solute, corresponding to subscript s, and solvent, corresponding to subscript w, into the differential control volume be zero. Therefore

$$\int_{-\frac{1}{2}h(x)}^{+\frac{1}{2}h(x)} (\rho_s u_s + \rho_w u_w)\, dy|_{x=x} - \int_{-\frac{1}{2}h(x+\Delta x)}^{+\frac{1}{2}h(x+\Delta x)} (\rho_s u_s + \rho_w u_w)\, dy|_{x=x+\Delta x} + [N(x) + F_s + F_w]\,\Delta x = 0, \quad (2.1)$$

where $N(x)$ is the total active solute mass flux per unit length and depth entering a symmetrical channel from the active transport sites, F_w is the total passive flux of water crossing the two lateral membranes owing to the local osmotic gradient and the rest of the notation is standard. The intercellular membranes are assumed, as in DB, to be semi-permeable, although the authors believe that this condition needs to be examined more critically, at least for the gall bladder. Thus, the passive solute flux F_s will be neglected.

The local mass average velocity u of the two-species system and the bulk density ρ are defined by

$$u = (\rho_s u_s + \rho_w u_w)/\rho, \quad \rho = \rho_s + \rho_w.$$

Using these definitions, dividing (2.1) by Δx and taking the limit as $\Delta x \to 0$, we obtain

$$-\frac{d}{dx}\int_{-\frac{1}{2}h(x)}^{+\frac{1}{2}h(x)} \rho u\, dy + N(x) + F_w = 0. \tag{2.2}$$

The bulk fluid density is related to the solute molar concentration C_s by

$$\rho = [M_s - (\bar{V}_s/\bar{V}_w)\, M_w]\, C_s + M_w/\bar{V}_w,$$

where M is the molecular weight and $\bar{V}$ the specific molar volume. As typical solute concentrations for the biological systems considered are of the order of 2×10^{-4} moles/ml the bulk fluid density is nearly independent of solute concentration. If an integral average velocity is defined as

$$\bar{u} = \frac{1}{h(x)}\int_{-\frac{1}{2}h(x)}^{+\frac{1}{2}h(x)} u\, dy$$

and ρ assumed constant, the overall continuity equation can be written in terms of this integral property as

$$\rho\, d(\bar{u}h)/dx = N(x) + F_w. \tag{2.3}$$

The passive water flux across an isothermal semi-permeable membrane separating two non-isotonic solute bathing solutions can be linearly related to the solute concentration difference across the membrane if the hydrostatic pressure differential across the membrane is not excessively large and if the concentrations of solute in the bathing solutions are low. Both these conditions are met in normal biological membranes. Equation (2.3) is therefore written as

$$\rho\, d(\bar{u}h)/dx = N(x) + 2P_w \delta C_s, \tag{2.4}$$

where P_w is a water permeability coefficient for the lateral membrane and $\delta C_s = C_{sw} - C_{s0}$ is the local discontinuity in solute concentration across the intercellular membrane, C_{sw} and C_{s0} being the solute concentrations at the membrane wall within the channel and in the cell interior respectively.

2.2. *Conservation of solute equation*

The derivation of the solute conservation relation for the differential control volume closely parallels that just performed for total mass conservation. The counterpart of (2.2) is obtained by replacing ρu by the solute flux $\rho_s u_s$. Requiring $F_s = 0$ and taking the limit as $\Delta x \to 0$ yields

$$\frac{d}{dx}\int_{-\frac{1}{2}h(x)}^{+\frac{1}{2}h(x)} \rho_s u_s\, dy = N(x). \tag{2.5}$$

The integrand of (2.5) can be represented as a sum of convective and diffusive solute fluxes by defining a diffusive streamwise solute flux J_{sx} relative to the mass average velocity u:

$$J_{sx} = \rho_s(u_s - u).$$

Equation (2.5) then becomes

$$\frac{d}{dx}\int_{-\frac{1}{2}h(x)}^{+\frac{1}{2}h(x)} M_s C_s u\, dy + \frac{d}{dx}\int_{-\frac{1}{2}h(x)}^{+\frac{1}{2}h(x)} J_{sx}\, dy = N(x). \tag{2.6}$$

An integral average convective solute flux $\overline{C_s u}$ and an integral average streamwise diffusive flux $\bar{J}_{sx}$ are now defined as

$$\overline{C_s u} = \frac{1}{h}\int_{-\frac{1}{2}h}^{+\frac{1}{2}h} C_s u \, dy, \quad \bar{J}_{sx} = \frac{1}{h}\int_{-\frac{1}{2}h}^{+\frac{1}{2}h} J_{sx} \, dy.$$

If pressure diffusion effects are neglected, the local streamwise diffusive flux is linearly related to the streamwise solute concentration gradient by

$$J_{sx} = -M_s \frac{\rho_w}{\rho} D \frac{\partial C_s}{\partial x}, \tag{2.7}$$

where D is the mass diffusivity for the solute.

Using the above definitions of the integral average properties, we can write the solute conservation equation (2.6) as

$$M_s \frac{d}{dx}(\overline{C_s u} h) + \frac{d}{dx}(\bar{J}_{sx} h) = N(x). \tag{2.8}$$

2.3. *Momentum equation*

An order-of-magnitude analysis of the steady-state Navier–Stokes momentum equations shows that these equations can be approximated by those for a quasi-unidirectional flow field provided that $(\rho U_0 h_0/\mu)\alpha \ll 1$ and $h_0/L \ll 1$, where U_0 is the characteristic streamwise velocity component, h_0 and L are the characteristic channel height and length respectively, α is a characteristic streamline slope and μ is the fluid viscosity. This condition is similar to that used in lubrication theory, where the usual Reynolds number is modified to take into account the small streamline inclination at boundaries. In the present context α must be generalized to include the effect of passive water movement and secretion at the channel boundaries. The above conditions are satisfied under most circumstances for extracellular channel transport with the possible exception of regions in close proximity to stagnation points within the channel. One would expect such regions of deviation from unidirectional flow to be limited to axial distances of only several channel heights and, therefore, not to significantly affect the flow behaviour on the larger length scale of the channel length L.

The momentum equation, therefore, requires that

$$\partial p/\partial y = 0, \tag{2.9}$$

$$\partial p/\partial x = \mu \, \partial^2 u/\partial y^2. \tag{2.10}$$

From (2.9), $p = p(x)$ and (2.10) can be integrated across the channel to give

$$h(x)\, dp/dx = \mu \left[\frac{\partial u}{\partial y}\right]_{y=-\frac{1}{2}h}^{y=+\frac{1}{2}h}, \tag{2.11}$$

where the right-hand side represents the sum of the shearing stresses at the upper and lower lateral boundaries.

2.4. *Continuity of flux at the lateral boundaries*

The diffusive flux of salt crossing the lateral boundaries of the channel must be consistent with the normal gradient of the solute concentration at these boundaries. Therefore at the lateral boundaries $y = \pm \frac{1}{2}h$

$$J_{sy} = -M_s \frac{\rho_w}{\rho} D \frac{\partial C_s}{\partial y} = \rho_s(v_s - v),$$

where v is the normal velocity component. The second equality on the right-hand side can be written in terms of the total solute and water fluxes crossing the upper lateral membrane:

$$\rho_s(v_s - v) = \frac{\rho_w}{\rho} \frac{N(x)}{2} - \frac{\rho_s}{\rho} \frac{F_w}{2}.$$

Combining these two results and the definition of the passive water flux $F_w = 2P_w \delta C_s$, one obtains

$$2M_s D \frac{\partial C_s}{\partial y} = N(x) - \frac{M_s C_s}{\rho_w} P_w \delta C_s \quad \text{at} \quad y = +\tfrac{1}{2}h. \tag{2.12}$$

2.5. *Dimensionless equations and parameters*

The four equations (2.4), (2.8), (2.11) and (2.12) constitute the basic conservation relations for the determination of the pressure, velocity and solute concentration in the channel. Additional insight into the qualitative behaviour of these equations can be had by casting them in dimensionless form and deducing the basic dimensionless groups that enter into the equations and boundary conditions. To this end all the variables in the problem are non-dimensionalized according to the following relations, the dimensionless variables being denoted by asterisks:

$$\left.\begin{aligned} h^* = h/h_0, \quad x^* = x/h_0, \quad y^* = y/h_0, \\ C_s^* = C_s/C_{s0}, \quad u^* = u/U_0, \quad p^* = P/P_0, \quad N^* = N/N_0. \end{aligned}\right\} \tag{2.13}$$

The quantities h_0 and N_0 represent some arbitrarily specified reference channel height and active solute flux, respectively, and C_{s0} is the concentration in the cell interior. The previously mentioned order-of-magnitude analysis of the momentum equation obviates the need to introduce separate x and y co-ordinate scalings. U_0 and P_0 are unknown and are to be determined by an appropriate balancing of terms in the governing equations. This non-dimensionalization procedure is equivalent to that performed for the DB equations by Segel (1970). The only difference is that Segel uses a streamwise co-ordinate scaling based on the secretory site length in place of the channel height.

Substitution of the relations (2.13) into (2.4), (2.8), (2.11) and (2.12) yields, after dividing by the coefficients of the first terms on the left-hand side of the equations:

$$\frac{d(\bar{u}^* h^*)}{dx^*} = \frac{N_0}{\rho U_0} N^* + \frac{2P_w \rho_{s0}}{M_s \rho U_0}(C_{sw}^* - 1), \tag{2.14}$$

$$\frac{d(\overline{C_s u^* h^*})}{dx^*} + \frac{D}{h_0 U_0}\frac{d(\overline{J^*_{sx}} h^*)}{dx^*} = \frac{N_0}{\rho_{s0} U_0} N^*, \tag{2.15}$$

$$2\frac{\partial C^*_s}{\partial y^*}\bigg|_{y^*=\frac{1}{2}h^*} = \frac{N_0 h_0}{\rho_{s0} D} N^* - \frac{P_w h_0 \rho_{s0}}{M_s D \rho} C^*_{sw}(C^*_{sw} - 1), \tag{2.16}$$

$$h^* \frac{dP^*}{dx^*} = \frac{\mu U_0}{p_0 h_0}\left[\frac{\partial u^*}{\partial y^*}\right]^{y=\frac{1}{2}h^*}_{y=-\frac{1}{2}h^*}, \tag{2.17}$$

where we have assumed that $\rho_w = \rho$, put $\rho_{s0} = C_{s0} M_s$ and defined the following non-dimensional average quantities:

$$\bar{u}^* = \bar{u}/U_0, \quad \overline{C_s u^*} = \overline{C_s u}/C_{s0} U_0,$$

$$\overline{J^*_{sx}} = -\frac{1}{h^*}\int_{-\frac{1}{2}h^*}^{\frac{1}{2}h^*} \frac{\partial C^*_s}{\partial x^*}\, dy^* = \frac{h_0}{\rho_{s0} D}\overline{J_{sx}}.$$

The dimensionless equations (2.14)–(2.17) are seen to contain seven dimensionless coefficient groups involving the five characteristic reference quantities. The number of independent groups can be reduced by the proper choice of the yet unspecified reference quantities U_0 and P_0. U_0 is chosen so that the coefficients of the convective and diffusive terms in (2.15) are equal. Setting $U_0 = D/h_0$ reduces the dimensionless coefficient of the diffusive term to unity and eliminates one of the dimensionless groups. The choice for P_0 is obvious since it appears in only one group. Setting P_0 equal to $\mu U_0/h_0$ in (2.17) eliminates one more dimensionless coefficient and makes the coefficients of the left- and right-hand sides of the equation both equal to unity. The remaining five dimensionless coefficients can now be redefined in terms of the three groups

$$\epsilon = \rho_{s0}/\rho, \quad \eta = N_0 h_0/\rho D, \quad R = P_w h_0/M_s D.$$

Substitution of these quantities into (2.14)–(2.17) yields

$$d(\bar{u}^* h^*)/dx^* = \eta N^* + 2\epsilon R(C^*_{sw} - 1), \tag{2.18}$$

$$\frac{d}{dx^*}(\overline{C_s u^*} h^*) + \frac{d}{dx^*}(\bar{J}^*_{sx} h^*) = \frac{\eta}{\epsilon} N^*, \tag{2.19}$$

$$2\frac{\partial C^*_s}{\partial y^*}\bigg|_{y^*=\frac{1}{2}h^*} = \frac{\eta}{\epsilon} N^* - \epsilon R C^*_{sw}(C^*_{sw} - 1), \tag{2.20}$$

$$h^* \frac{dP^*}{dx^*} = \left[\frac{\partial u^*}{\partial y^*}\right]^{y^*=\frac{1}{2}h^*}_{y^*=-\frac{1}{2}h^*}. \tag{2.21}$$

The dimensionless group η represents the ratio of the active transport flux of solute to the convective flux of water, while R is a measure of the ratio of the passive flux of water across the lateral boundaries to the convective flux of solute. The third parameter ϵ is simply a measure of the solute concentration in the cell interior. The boundary conditions introduce five additional dimensionless groups: $C^*_s(0) = C_s(0)/C_{s0}$ and $C^*_s(L) = C_s(L)/C_{s0}$, representing the solute concentration at the two ends of the channel; $L^* = L/h_0$, the dimensionless channel length; $U(0)^* = U(0)/U_0$, a dimensionless entrance velocity in an open geometry channel; and a dimensionless secretory site length $\Delta l/h_0$.

For a given channel, we specify the values for h_0, L, D, P_w, ρ, ρ_{s_0} and M_s and, thereby, the values of η, ϵ and R. In a closed-geometry channel, where the mass flux and axial solute concentration gradient both vanish at the closed end, only $C_s^*(L)$ or $C_s^*(0)$ remains as a free parameter to satisfy the boundary-value problem. For open-geometry channels, three degrees of freedom, $U^*(0)$, $C_s^*(0)$ and $C_s^*(L)$, are available to satisfy end conditions for solute concentration and hydrodynamic pressure differential.

2.6. *Velocity and concentration profiles*

Equations (2.18)–(2.21) permit us to define at most three profile coefficients for the description of the velocity and solute concentration fields. The fourth unknown function of x is the pressure. If we assume that the passive water flux produces only small departures from the no-slip boundary condition at the lateral boundaries and that the fluid viscosity is uniform across the channel, the order-of-magnitude analysis of the Navier–Stokes momentum equation mentioned previously suggests that a one-parameter Poiseuille-like parabolic velocity profile is appropriate for the extracellular channel flow. It is assumed, therefore, that the velocity profile is of the form

$$u^*(x, y) = U_m^*(x)\,[1-(2y^*/h^*)^2].$$

This profile family satisfies (2.9), (2.10) and the no-slip boundary condition, and allows the centre-line velocity U_m, and hence the bulk flow, to vary as a function of x.

For the solute concentration profile a two-parameter family was selected in terms of the dimensionless concentration C_{sw}^* at the lateral boundary and the centre-line concentration C_{sm}^*. This permits an estimate of the rate of mixing across the channel and provides an independent measure of the local osmotic effect along the lateral boundary. A convenient profile that allows the two parameters C_{sw}^* and C_{sm}^* to vary in a continuous manner along the channel is the quadratic form

$$C_s^* = C_{sw}^* + (C_{sm}^* - C_{sw}^*)\,[1-(2y^*/h^*)^2].$$

2.7. *Equations for the profile coefficients and pressure*

The dimensionless integral average properties can now be expressed in terms of the three profile coefficients introduced in the last subsection as follows:

$$\overline{u}^* = \frac{2}{h^*}\int_0^{\frac{1}{2}h^*} u^*\,dy^* = \tfrac{2}{3}U_m^*(x),$$

$$\overline{C_s u^*} = \frac{2}{h^*}\int_0^{\frac{1}{2}h^*} (C_s^* u^*\,dy) = \tfrac{6}{5}U_m^* C_{sw}^* - \tfrac{8}{15}U_m^* C_{sm}^*,$$

$$\bar{J}_{sx}^* = -\left(\frac{2}{3}\frac{dC_{sm}^*}{dx^*} + \frac{1}{3}\frac{dC_{sw}^*}{dx^*}\right).$$

Substitution of these expressions into (2.18)–(2.21) yields, with asterisks omitted,

$$\frac{2}{3}\frac{d(U_m h)}{dx} = \eta N + 2\epsilon R(C_{sw}-1), \tag{2.22}$$

$$\frac{6}{5}\frac{d}{dx}(U_m C_{sw} h) - \frac{8}{15}\frac{d}{dx}(U_m C_{sm} h) - \frac{d}{dx}\left(\frac{2h}{3}\frac{dC_{sm}}{dx} + \frac{h}{3}\frac{dC_{sw}}{dx}\right) = \frac{\eta}{\epsilon}N, \tag{2.23}$$

$$\frac{8}{h}(C_{sw} - C_{sm}) = \frac{\eta}{\epsilon}N - \epsilon R C_{sw}(C_{sw} - 1), \tag{2.24}$$

$$dP/dx = -8U_m/h^2. \tag{2.25}$$

In presenting the results it will be convenient to refer to the dimensionless volume flux Q^* at any station rather than U_m and to introduce a dimensionless total solute flux Q_s^*. From the three expressions for the integral average properties above

$$Q^* = \int_{-\frac{1}{2}h^*}^{\frac{1}{2}h^*} u^* \, dy^* = \tfrac{2}{3}U_m^*(x)\, h^*(x) \tag{2.26a}$$

and $$Q_s^* = \bar{J}_{sx}^* h^* + \overline{C_s u^*} h^* = U_m^* h^* \left(\frac{6C_{sw}^*}{5} - \frac{8C_{sm}^*}{15}\right) - h^* \left(\frac{2}{3}\frac{dC_{sm}^*}{dx^*} + \frac{1}{3}\frac{dC_{sw}^*}{dx^*}\right), \tag{2.26b}$$

where again the asterisk will be dropped from now on.

3. Approximate analytic solutions

Equations (2.22), (2.23), (2.24) and (2.25) provide a coupled system of one algebraic and three ordinary differential equations for the three profile coefficients C_{sm}, C_{sw}, U_m and the pressure. Numerical solutions to various split-end-point boundary-value problems associated with these four equations are presented in §§ 5 and 6. Our objective here is to see if approximate analytic solutions can be obtained for physiologically meaningful simplifications of the system (2.22)–(2.25). To this end, one notes that for the extracellular channels in the ciliary body epithelium both η and R are of order 10^{-3} or smaller, values being based on the best available estimates of the quantities included in these dimensionless coefficients. For these conditions the right-hand side of (2.24) is very much less than one and $C_{sw} \approx C_{sm}$. Thus, the necessary conditions for the validity of the instantaneous mixing hypothesis used in DB, in which a uniform concentration profile across the channel with $C_s = C_{sw} = C_{sm}$ is assumed, is that $\eta/\epsilon, \epsilon R \ll 1$. This hypothesis is reasonable for the ciliary body and the gall bladder, but probably not valid for short extracellular channels such as the intracellular canaliculi of the small intestine.

Two additional simplifications that greatly reduce the difficulty of the analysis without altering the basic physics are to let the channel height be constant ($h = 1$) and to treat the active transport site as a point rather than a distributed solute source. If this source is located at $x = L_s$, then for $x \neq L_s$ equations (2.22), (2.23) and (2.25) reduce to

$$dQ/dx = 2\epsilon R(C_s - 1), \tag{3.1}$$

$$\frac{d}{dx}(QC_s) - \frac{d^2C_s}{dx^2} = 0, \quad \frac{dP}{dx} = -12Q, \tag{3.2), (3.3}$$

while the source strength S is defined by

$$S = \int_{L_s^-}^{L_s^+} \frac{\eta}{\epsilon} N \, dx, \tag{3.4}$$

where $L_s^- \to L_s^+$. The matching conditions at the solute source are

$$P(L_s^+) = P(L_s^-), \quad C_s(L_s^+) = C_s(L_s^-), \quad Q(L_s^+) - Q(L_s^-) = \epsilon S, \tag{3.5a–c}$$

$$\frac{dC_s}{dx}(L_s^+) - \frac{dC_s}{dx}(L_s^-) = -S + \epsilon S C_s(L_s), \tag{3.5d}$$

where the last two conditions are obtained by integrating (2.22) and (2.23) across the secretory site and then applying the limiting process $L_s^- \to L_s^+$ for a point source. We observe from (3.5d) that the secretory site produces a discontinuity in concentration gradient at the source location, its magnitude to lowest order being proportional to the source strength.

The boundary conditions at the channel entrance and exit are

$$C_s(0) = C(0), \quad C_s(L) - C_s(0) = \Delta C, \quad P(L) - P(0) = \Delta P, \tag{3.5e,f,g}$$

$$P = P(0) \quad \text{at} \quad x = 0, \tag{3.5h}$$

where $C(0)$, ΔC, $P(0)$ and ΔP are prescribed.

The simplified system of equations (3.1)–(3.3) is still not easy to solve because of the nonlinear coupling between Q and C_s. This last difficulty can be handled readily, however, if the concentration field is only weakly coupled to the filtration flow and local osmotic water movement, that is if ΔP and $\epsilon R \ll 1$. We therefore develop C_s, Q and P as a double perturbation expansion in integral powers of ϵR and ΔP. This expansion has the effect of separating out, to first order, the convective corrections for the filtration flow produced by the externally applied pressure differential ΔP and the passive water movement across the lateral boundaries due to local osmosis.

$$\left.\begin{aligned} C_s &= C^{(0)} + \epsilon R C_1^{(1)} + \Delta P C_2^{(1)} + \ldots, \\ Q &= Q^{(0)} + \epsilon R Q_1^{(1)} + \Delta P Q_2^{(1)} + \ldots, \\ P &= P^{(0)} + \epsilon R P_1^{(1)} + \Delta P P_2^{(1)} + \ldots. \end{aligned}\right\} \tag{3.6}$$

The series solutions denoted by (3.6) will not in general be uniformly valid for large x unless the independent variable x is strained. This complication occurs because the range of the x integration, which is the channel length L, is $\gg 1$ and can give rise to first-order convective corrections $\epsilon R C_1^{(1)}$ and $\Delta P C_2^{(1)}$ which can be of the same order or larger than $C^{(0)}$. Inspection of (3.1)–(3.3) shows that such secular behaviour can be anticipated if $Q \geqslant O(1)$, Q being of $O(\epsilon RL)$. To avoid this undesirable growth of the solution (3.6) for $x \gg 1$ we introduce a two-parameter PLK type co-ordinate expansion:

$$x = x_0 + \epsilon R x_1(x_0) + \Delta P x_2(x_0) + \ldots. \tag{3.7}$$

The unknown functions $C_i^{(j)}$, $Q_i^{(j)}$ and $P_i^{(j)}$ appearing in (3.6) are now considered as functions of the strained co-ordinate x_0 and are obtained by solving the differential equations which are obtained when (3.6) and (3.7) are substituted into (3.1)–(3.3) and coefficients of like order in ϵR and ΔP are equated.

To zeroth order:

$$dP^{(0)}/dx_0 = -12Q^{(0)}, \tag{3.8a}$$

$$\frac{d}{dx_0}(Q^{(0)}C^{(0)}) - \frac{d^2C^{(0)}}{dx_0^2} = 0, \tag{3.8b}$$

$$dQ^{(0)}/dx_0 = 0. \tag{3.8c}$$

To first order in ϵR:

$$\frac{dP_1^{(1)}}{dx_0} - \frac{dx_1}{dx_0}\frac{dP^{(0)}}{dx_0} = -12Q_1^{(1)}, \tag{3.9a}$$

$$\frac{d^2C_1^{(1)}}{dx_0^2} = \frac{d}{dx_0}[Q^{(0)}C_1^{(1)} + Q_1^{(1)}C^{(0)}] - \frac{dx_1}{dx_0}\frac{d}{dx_0}[Q^{(0)}C^{(0)}] + 2\frac{dx_1}{dx_0}\frac{d^2C^{(0)}}{dx_0^2} + \frac{d^2x_1}{dx_0^2}\frac{dC^{(0)}}{dx_0}, \tag{3.9b}$$

$$\frac{dQ_1^{(1)}}{dx_0} - \frac{dx_1}{dx_0}\frac{dQ^{(0)}}{dx_0} = 2(C^{(0)} - 1). \tag{3.9c}$$

To first order in ΔP:

$$\frac{dP_2^{(1)}}{dx_0} - \frac{dx_2}{dx_0}\frac{dP^{(0)}}{dx_0} = -12Q_2^{(1)}, \tag{3.10a}$$

$$\frac{d^2C_2^{(1)}}{dx_0^2} = \frac{d}{dx_0}[Q^{(0)}C_2^{(1)} + Q_2^{(1)}C^{(0)}] - \frac{dx_2}{dx_0}\frac{d}{dx_0}[Q^{(0)}C^{(0)}] + 2\frac{dx_2}{dx_0}\frac{d^2C^{(0)}}{dx_0^2} + \frac{d^2x_2}{dx_0^2}\frac{dC^{(0)}}{dx_0}, \tag{3.10b}$$

$$\frac{dQ_2^{(1)}}{dx_0} - \frac{dx_2}{dx_0}\frac{dQ^{(0)}}{dx_0} = 0. \tag{3.10c}$$

Equations (3.8), (3.9) and (3.10) each constitute a system of six ordinary differential equations: three for the range $0 < x < L_s$ and three for the range $L_s < x < L$, whose total order is eight. The eight unknown integration constants are determined for each of the systems (3.8), (3.9) and (3.10) by the eight boundary and matching conditions that are obtained by substituting (3.6) and (3.7) into (3.5) and equating coefficients of each power of ϵR and ΔP. The boundary conditions for the lowest order set of equations, equations (3.8), are homogeneous for P and inhomogeneous for C_s, assuming ΔC is of $O(1)$, while for the first-order set (3.9) the boundary conditions on both P and C_s are homogeneous. For the first-order set (3.10) the pressure boundary condition is inhomogeneous since it introduces the filtration pressure differential ΔP. With this ordering the total contributions to the water flux Q from osmosis, active transport and filtration can be of comparable magnitude.

For each higher order system one has to solve an auxiliary second-order differential equation for the co-ordinate straining functions x_i in the two regions $0 < x < L_s$ and $L_s < x < L$. The differential equations for x_1 and x_2 are determined by suppressing the undesirable growth that results from the inhomogeneous terms in (3.9*b*) and (3.10*b*). These terms lead to solutions for $C_1^{(1)}$ and $C_2^{(1)}$ which exhibit a monotonically increasing algebraic growth for values of $x \gg 1$, and consequently a divergence of the series (3.6) for large x. To suppress this secular behaviour one requires instead that $C_1^{(1)}$ and $C_2^{(1)}$ should satisfy the homogeneous equations

$$\frac{d^2C_1^{(1)}}{dx_0^2} = 0, \quad \frac{d^2C_2^{(1)}}{dx_0^2} = 0 \quad \text{for} \quad 0 < x_0 < L_{0s} \quad \text{and} \quad L_{0s} < x_0 < L_0, \tag{3.11a}$$

which are obtained by making the unknown functions x_1 and x_2 in (3.9*b*) and (3.10*b*) obey

$$\frac{d^2x_{1,2}}{dx_0^2}\frac{dC^{(0)}}{dx_0} + \frac{dx_{1,2}}{dx_0}\left[2\frac{d^2C^{(0)}}{dx_0^2} - \frac{d}{dx_0}Q^{(0)}C^{(0)}\right] + \frac{d}{dx_0}[Q^{(0)}C_{1,2}^{(1)} + Q_{1,2}^{(1)}C^{(0)}] = 0, \tag{3.11b}$$

where L_0 represents the value of the x_0 co-ordinate at the channel exit. The boundary and matching conditions for the unknown functions x_1 and x_2 are to some extent arbitrary. At $x_0 = L_{0s}$, the source location in the strained co-ordinate system, it is reasonable to require that the strained co-ordinate be continuous and that the compatibility condition (3.5*d*) be satisfied to first order in ϵR and ΔP:

$$x_1(L_{0s}^-) = x_1(L_{0s}^+), \quad x_2(L_{0s}^-) = x_2(L_{0s}^+), \tag{3.12a}$$

$$\left[\frac{dC_1^{(1)}}{dx_0} - \frac{dx_1}{dx_0}\frac{dC^{(0)}}{dx_0}\right]_{x_0 = L_{0s}^+} = \left[\frac{dC_1^{(1)}}{dx_0} - \frac{dx_1}{dx_0}\frac{dC^{(0)}}{dx_0}\right]_{x_0 = L_{0s}^-} + \frac{S}{R}C^{(0)}(L_{0s}), \tag{3.12b}$$

$$\left[\frac{dC_2^{(1)}}{dx_0} - \frac{dx_2}{dx_0}\frac{dC^{(0)}}{dx_0}\right]_{x_0 = L_{0s}^+} = \left[\frac{dC_2}{dx_0} - \frac{dx_2}{dx_0}\frac{dC^{(0)}}{dx_0}\right]_{x_0 = L_{0s}^-}. \tag{3.12c}$$

Equations (3.11*b*) are of second order and thus permit the specification of two additional conditions. For compatability with (3.2) and (3.5*b*) we must have

$$\left.\frac{dx_1}{dx_0}\right|_{x_0 = L_{0s}^-} = \left.\frac{dx_1}{dx_0}\right|_{x_0 = L_{0s}^+}, \qquad \left.\frac{dx_2}{dx_0}\right|_{x_0 = L_{0s}^-} = \left.\frac{dx_2}{dx_0}\right|_{x_0 = L_{0s}^+}, \tag{3.12d}$$

and for convenience we choose

$$x_1(0) = x_2(0) = 0. \tag{3.12e}$$

For $C_1^{(1)}$ and $C_2^{(1)}$ to be zero for all x_0 and to satisfy (3.11*a*), $C_1^{(1)}$ and $C_2^{(1)}$ must obey homogeneous boundary and matching conditions. The first-order conditions derived from (3.5*b*,*e*,*f*) and (3.12*b*,*c*) will satisfy this homogeneity requirement provided that

$$\left.\frac{dC_{1,2}^{(1)}}{dx_0}\right|_{x_0 = L_{0s}^-} = \left.\frac{dC_{1,2}^{(1)}}{dx_0}\right|_{x_0 = L_{0s}^+}$$

in (3.12*b*,*c*). In this manner the undesirable growth of the dependent variables is eliminated through the co-ordinate straining functions. With the conditions (3.12) we are not free to specify the values of x_0 at the secretory site and at the channel exit; these are determined from a solution of the two simultaneous equations which are obtained when $x = L_s$ and $x = L$ in (3.7). These equations, which are implicit algebraic relations for L_{0s} and L_0, must be solved numerically.

The zeroth-order volume flux gradient $dQ^{(0)}/dx_0$ vanishes by (3.8*c*) and the zeroth-order pressure gradient $dP^{(0)}/dx_0$ vanishes after solving (3.8*a*, *c*) with appropriate boundary conditions. The first-order pressure and volume flux gradients in (3.9*a*, *c*) and (3.10*a*, *c*) are then independent of the co-ordinate straining as represented by dx_1/dx_0 and dx_2/dx_0, and depend only on the zeroth-order concentration solution. However, the co-ordinate straining does enter into the second-order volume flux corrections $Q_{1,2}^{(2)}$ and pressure corrections $P_{1,2}^{(2)}$, which are derived from (3.2) and (3.3).

To order $(\epsilon R)^2$ and $(\Delta P)^2$

$$\frac{dQ_{1,2}^{(2)}}{dx_0} = \frac{dQ_{1,2}^{(1)}}{dx_0}\frac{dx_{1,2}}{dx_0}, \quad \frac{dP_{1,2}^{(2)}}{dx_0} = -12Q_{1,2} + \frac{dP_{1,2}^{(1)}}{dx_0}\frac{dx_{1,2}}{dx_0}. \tag{3.13}$$

Zeroth-order solution. The solution of (3.8) and the associated boundary and matching conditions are

$$P^{(0)} = P(0), \quad Q^{(0)} = 0, \tag{3.14a,b}$$

$$C^{(0)} = \left[\frac{\Delta C}{L_0} + \left(1 - \frac{L_{0s}}{L_0}\right) S\right] x_0 + C(0) \quad (0 < x_0 < L_{0s}), \tag{3.14c}$$

$$C^{(0)} = \left(\frac{\Delta C}{L_0} - \frac{L_{0s}}{L_0} S\right) x_0 + C(0) + SL_{0s} \quad (L_{0s} < x_0 < L_0). \tag{3.14d}$$

The lowest order solution thus involves no convective transport. This solution is simply a linear variation in concentration due to solute diffusion between two specified end states, with a discontinuity in solute concentration gradient at the secretory site location $x_0 = L_{0s}$ whose magnitude is proportional to the source strength S. This basic behaviour is clearly suggested by the curves in figure 7 below.

Solution to first order in ϵR. To solve (3.9) we first integrate (3.9*c*) for $0 < x_0 < L_{0s}$ and $L_{0s} < x_0 < L_0$ using (3.14). The integration constants in the resulting expressions for $Q_1^{(1)}$ cannot be evaluated directly since they are related to the pressure boundary conditions. The expressions for $Q_1^{(1)}$ are therefore substituted in (3.9*a*). The integral of (3.9*a*) leads to two relations for $P_1^{(1)}$ valid for $0 < x_0 < L_{0s}$ and $L_{0s} < x_0 < L_0$ with four unknown constants. The latter are evaluated by applying the four appropriate first-order boundary and matching conditions that are derived from (3.5*a*, *c*, *g*, *h*). The desired expressions for $Q_1^{(1)}$ and $P_1^{(1)}$ valid in each region are

$$Q_1^{(1)} = \alpha_1 x_0^2 + 2(C(0) - 1) x_0 + \alpha_3 \quad (0 < x_0 < L_{0s}), \tag{3.15a}$$

$$Q_1^{(1)} = \alpha_2 x_0^2 + 2(C(0) + SL_{0s} - 1) x_0 + \alpha_4 \quad (L_{0s} < x_0 < L_0), \tag{3.15b}$$

$$P_1^{(1)} = -12[\tfrac{1}{3}\alpha_1 x_0^3 + (C(0) - 1) x_0^2 + \alpha_3 x_0] \quad (0 < x_0 < L_{0s}), \tag{3.15c}$$

$$P_1^{(1)} = -12[\tfrac{1}{3}\alpha_2 x_0^3 + (C(0) + SL_{0s} - 1) x_0^2 + \alpha_4 x_0] \quad (L_{0s} < x_0 < L_0), \tag{3.15d}$$

where

$$\alpha_1 = \Delta C/L_0 + (1 - L_{0s}/L_0) S, \quad (\alpha_2 = \alpha_1 - S),$$

$$\alpha_3 = -(1 - L_{0s}/L_0)(S/R + \tfrac{1}{3} SL_{0s}(2L_0 - L_{0s}) - (C(0) + \tfrac{1}{3}\Delta C - 1) L_0,$$

$$\alpha_4 = \alpha_3 + S/R - SL_{0s}^2.$$

Note that the first-order boundary-value problems for the pressure and water flux have been uncoupled from that for the concentration field. Equations (3.15*a*) and (3.15*b*) are the first-order approximations for the convective fluxes that would be produced in a channel with passive water movement due to local osmosis at its lateral boundaries and no transmembrane pressure differential and is based on the lowest order solution for the concentration distribution (3.14). The pressure distribution (3.15*c*, *d*) is the passively induced pressure field created by the local osmosis.

In view of (3.14*b*), (3.11*b*) reduces to an inhomogeneous second-order differential equation for x_1 alone:

$$\frac{d^2 x_1}{dx_0^2} \frac{dC^{(0)}}{dx_0} + \frac{d}{dx_0}(Q_1^{(1)} C^{(0)}) = 0, \tag{3.16}$$

where $C^{(0)}$ and $Q_1^{(1)}$ are given by (3.14*c*, *d*) and (3.15*a*, *b*) respectively. The integration of (3.16) in the two regions $0 < x_0 < L_{0s}$ and $L_{0s} < x_0 < L_0$ introduces a total of four unknown constants. These constants are evaluated by applying the four first-order boundary and matching conditions associated with (3.12). The final results are

$$x_1 = \frac{\alpha_5}{\alpha_1}x_0 - \frac{\alpha_1}{4}x_0^4 - [C(0) - \tfrac{2}{3}]x_0^3 - \left(\frac{2C(0)\,[C(0)-1]}{\alpha_1} + \alpha_3\right)\frac{x_0^2}{2} - \frac{\alpha_3 C(0)}{\alpha_1}x_0$$
$$(0 < x_0 < L_{0s}), \quad (3.17a)$$

$$x_1 = \frac{\alpha_5}{\alpha_2}x_0 - \frac{\alpha_2}{4}x_0^4 - [C(0) + SL_{0s} - \tfrac{2}{3}]x_0^3 - \left(\frac{2(C(0)+SL_{0s})\,(C(0)+SL_{0s}-1)}{\alpha_2} + \alpha_4\right)\frac{x_0^2}{2}$$
$$- \frac{\alpha_4(C(0)+SL_{0s})}{\alpha_2}x_0 - \alpha_6 \quad (L_{0s} < x_0 < L_0), \quad (3.17b)$$

where

$$\alpha_5 = \frac{1}{\alpha_2 - \alpha_1}\Big\{-\alpha_1\alpha_2\left(SL_{0s}^3 + \frac{S}{R}L_{0s}\right) + [2\alpha_2 C(0)\,(C(0)-1) - 2\alpha_1(C(0)+SL_{0s})$$
$$\times (C(0)+SL_{0s}-1)]\,L_{0s} + \alpha_2\alpha_3 C(0) - \alpha_1\alpha_4(C(0)+SL_{0s})\Big\},$$

$$\alpha_6 = \alpha_5 L_{0s}\left(\frac{\alpha_1-\alpha_2}{\alpha_1\alpha_2}\right) - \frac{SL_{0s}^4}{4}$$
$$+ \left[\frac{2C(0)\,(C(0)-1)}{\alpha_1} - \frac{2(C(0)+SL_{0s})\,(C(0)+SL_{0s}-1)}{\alpha_2} - \frac{S}{R}\right]\frac{L_{0s}^2}{2}$$
$$+ \left[\frac{\alpha_3 C(0)}{\alpha_1} - \frac{\alpha_4(C(0)+SL_{0s})}{\alpha_2}\right]L_{0s}.$$

Solution to first order in ΔP. The solutions to (3.10) are obtained in a manner exactly analogous to that used to obtain the results to first order in ϵR. After integration and application of appropriate boundary and matching conditions we obtain

$$Q_2^{(1)} = -1/12L_0, \quad P_2^{(1)} = x_0/L_0. \quad (3.18a, b)$$

The straining function is found to be

$$x_2 = \frac{\alpha_7}{\alpha_1}x_0 + \frac{1}{12L_0}\left(\frac{x_0^2}{2} + \frac{C(0)}{\alpha_1}x_0\right) \quad (0 < x_0 < L_{0s}), \quad (3.19a)$$

$$x_2 = \frac{\alpha_7}{\alpha_2}x_0 + \frac{1}{12L_0}\left(\frac{x_0^2}{2} + \frac{C(0)+SL_{0s}}{\alpha_2}x_0\right) + \alpha_8 \quad (L_{0s} < x_0 < L_0), \quad (3.19b)$$

where

$$\alpha_7 = \frac{\alpha_1(C(0)+SL_{0s}) - \alpha_2 C(0)}{12L_0(\alpha_2-\alpha_1)},$$

$$\alpha_8 = \alpha_7 L_{0s}\left(\frac{\alpha_2-\alpha_1}{\alpha_1\alpha_2}\right) + \frac{1}{12L_0}\left[\frac{C(0)}{\alpha_1} - \frac{C(0)+SL_{0s}}{\alpha_2}\right]L_{0s}.$$

The solutions to second order in $(\epsilon R)^2$ are obtained by using the results (3.15) and (3.17) in (3.13) and applying the appropriate second-order boundary and matching conditions from (3.5). The detailed results are contained in Goldgraben (1972).

The approximate analytic solutions given above will be compared with the exact solutions of (2.22)–(2.25) in § 5 for circumstances in which $\Delta P = 0$.

4. Results for closed extracellular channels

The boundary-value problem for extracellular channels with impermeable junctional complexes at the luminal end $x = 0$, for example, the gall bladder geometry shown in figure 1, is readily converted into an initial-value problem in which equations (2.22), (2.23) and (2.25) are integrated numerically. C_{sm} and its derivatives are related to C_{sw} and its derivatives by the algebraic relation (2.24). Since $U_m(0) = 0$, $dC_{sw}(0)/dx = 0$ and the initial reference pressure is arbitrary, only one initial condition, the dimensionless initial concentration $C_{sw}(0)$, is left unspecified. In both DB and Segel (1970) $C_{sw}(0)$ is uniquely determined by requiring that $C_{sw} = 1$. However, for reasons stated earlier this isotonic exit condition is an artificial one. $C_{sw}(1)$ can have any value, depending on the mixing process that occurs between the channel effluent and the outer bathing solution. The boundary condition for determining $C_{sw}(0)$ is more properly applied at infinity, where the solution is collected and the concentration uniform. This equilibrium concentration is given by $C_\infty = Q_s/Q$.

To examine the entire spectrum of possible behaviour, $C_{sw}(0)$ will be treated as a free parameter in the present study. In particular we shall want to see if it is possible within the framework of the local standing-gradient osmotic model as presently formulated to have both a channel concentration which is hypotonic relative to the cell interior solution and a vanishing concentration gradient at the exit station. As discussed in § 1, both conditions appear to be necessary if the water in the cell interior is to be replenished from the lumen with the channel effluent and outer bathing solution both still being isotonic relative to the lumenal fluid.

The unexpected result in figure 4(*a*) is that concentration in the channel does not automatically relax to the concentration in the cell interior as the perfusion length for passive water movement increases. One observes that there is only one initial solute concentration C_{cr} at $x = 0$ that permits C_{sw} to approach unity asymptotically with vanishing gradient at large values of x. The dashed curve in figure 4 representing this unique solution curve separates two families of solutions with distinctly different behaviour. For $C_{sw}(0) > C_{cr}$, curves 1–3 in figure 4(*a*), C_{sw} eventually grows without bound for large values of x and leads to a monotonically increasing water flux in the channel. For $C_{sw}(0) < C_{cr}$, curves 4 and 5 in figure 4(*a*), C_{sw} decays monotonically towards zero for increasing values of x. Once $C_{sw} < 1.0$ water diffuses back into the cell interior and a reversal in flow direction will occur if the channel is sufficiently long, as shown by curve 5 of figure 4(*b*). One notes from figure 4 that only solutions of the type of curves 4 and 5 are possible if the exit boundary condition $C_{sw}(L) = 1$ is imposed as in DB and Segel. The solution curves for other values of η, ϵ and R in the range of interest for epithelial membranes all exhibit the same qualitative behaviour as that shown in figure 4. Varying these dimensionless groups simply alters the value of C_{cr} and changes the decay rate of the neutral (dashed) curve.

We next wish to interpret these results in the context of Diamond's (1964) experiments. If the effluent is to be isotonic with a well stirred outer bathing solution whose dimensionless far-field concentration is C_∞ then the channel flow

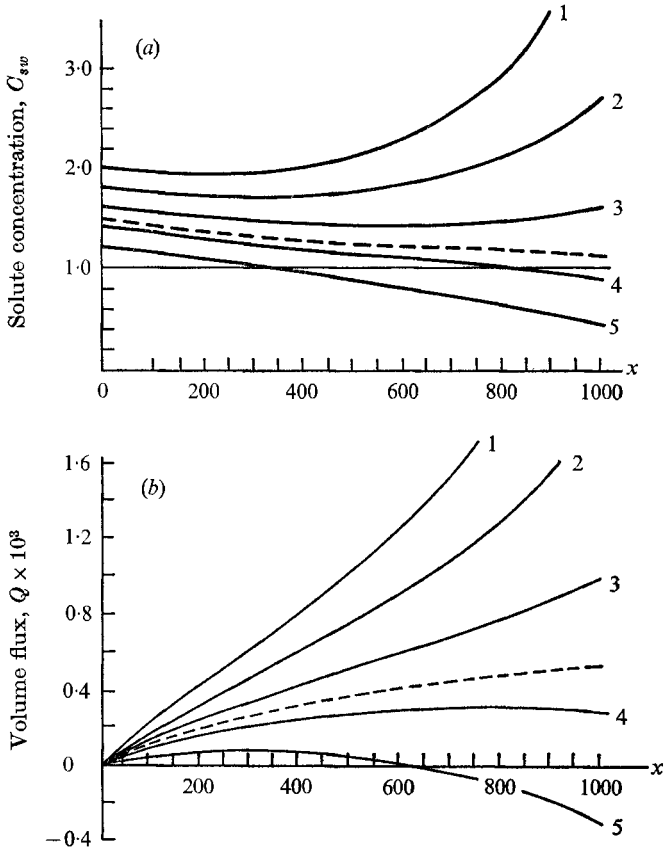

FIGURE 4. Effect of $C_{sw}(0)$ on (*a*) the distribution of solute concentration and (*b*) volume flux in a closed extracellular channel with the secretory site located in $0 < x < 50$. $\epsilon = 0{\cdot}872 \times 10^{-2}$, $\eta = 0{\cdot}135 \times 10^{-6}$, $R = 0{\cdot}116 \times 10^{-3}$. – – –, C_{cr}.

must reach the exit with both $C_{sw}(L) = C_\infty$ and $dC_{sw}(L)/dx = 0$, or further mixing would ensue at the channel exit. It is evident from figure 4(*a*) that when $C_{sw}(L) = C_\infty = 1$ only the dashed curve for the infinitely long channel satisfies both exit boundary conditions. Other solutions with a vanishing gradient at the channel exit are possible for finite-length channels. These solutions are represented by the curves of the upper family in figure 4(*a*) where the channel exit is located at the minima, $dC_{sw}/dx = 0$. Thus, if $L = 625$ then curve 3 terminated at $x = 625$ would represent such a solution. These solutions all correspond to an outer bathing solution which is hypertonic relative to the cell interior, that is $C_\infty = C_{sw}(L) > 1$. No mention has yet been made of the concentration of the lumenal fluid, however, if the water in the cell interior is to be replenished from the lumen, as is widely assumed, then the lumenal fluid must be hypotonic relative to the cell interior. This is the basic paradox of the standing-gradient model in the explanation of isotonic transport in the gall bladder. The solution in the cell interior, assuming homogeneity of cell water activity, obviously cannot at the same time be isotonic or hypotonic with respect to the outer bathing solution and hypertonic relative to the lumenal solution if these two bathing

solutions are isotonic. Also, there are no values of $C_{sw}(0)$ which allow the curves of the lower family in figure 4(*a*) to have a minimum with $C_{sw} < 1$. It would appear that basic modifications of the existing mathematical formulation are necessary if the conditions for both isotonic transport and water replenishment are to be explained using the local standing-gradient osmotic concept for gall bladder epithelial transport.

The question as to how long a channel would be required for the channel flow to nearly equilibrate with the solution in the cell interior has been examined in detail in DB and Segel (1970). While such equilibration ($C_{sw}(L) = 1$ and $dC_{sw}(L)/dx = 0$) cannot be exactly achieved for any finite-length channel, these investigators have demonstrated that, provided the solution curves are of the type 4 or 5 in figure 4, the equilibration can be approached to within a few per cent for estimated values of η, ϵ, R and L that are reasonable for gall bladder epithelium.

5. Results for porous extracellular channels

The initial-value problem for open and partially occluded extracellular channels with active transport is somewhat more difficult to handle numerically than the closed channel geometry just considered. In the case of channels completely occluded at one end, both U_m and the concentration gradient dC_{sw}/dx at the initial station are zero. Only the initial concentration $C_{sw}(0)$ is unknown. All three initial conditions are unknown in open channel systems. The two additional unknown initial conditions $U_m(0)$ and $dC_{sw}(0)/dx$ are related to the pressure difference $\Delta P = P(L) - P(0)$ and concentration difference $\Delta C_{sw} = C_{sw}(L) - C_{sw}(0)$ across the channel, see boundary conditions (3.5*f*, *g*). Thus, to integrate (2.22), (2.23) and (2.25) numerically trial values of $U_m(0)$ and $dC_{sw}(0)/dx$ had to be assumed and a variant of a steepest-descent iteration routine used to satisfy the split-end-point boundary conditions on pressure and concentration. Solutions were assumed to have converged to the desired accuracy when the prescribed values of ΔP and ΔC_{sw} were satisfied to five significant digits.

To understand the essential features of the operation of an open channel with active transport and pressure filtration we first consider an idealized constant-area channel with a secretory site centred symmetrically between the channel ends, which are at the same concentration as the cell interior, see figure 5. Curve 1 in figure 5(*a*) and curve 1 in figure 5(*b*) show the variation of dimensionless pressure P and volume flux Q when there is no applied pressure differential ΔP across the end stations. Water that enters the channel passively owing to local osmosis divides at the centre into two equal and oppositely directed flows. Since both Q and the concentration gradient vanish at the channel centre-line because of symmetry, the flux conditions at the symmetry plane of the channel are the same as those at the initial station of a tight-junction channel. Curves 2–4 in figures 5(*a*) and (*b*) show the effect of applying a monotonically increasing pressure differential across the membrane. An increase in the hydrodynamic pressure at the left-hand end over that at the right, with $\Delta C_{sw} = 0$, will cause the locations at which $Q = 0$ to move to the left as shown in figure 5(*b*). This position of the stagnation plane (i.e. $Q = 0$) is also the plane of maximum pressure, see equation

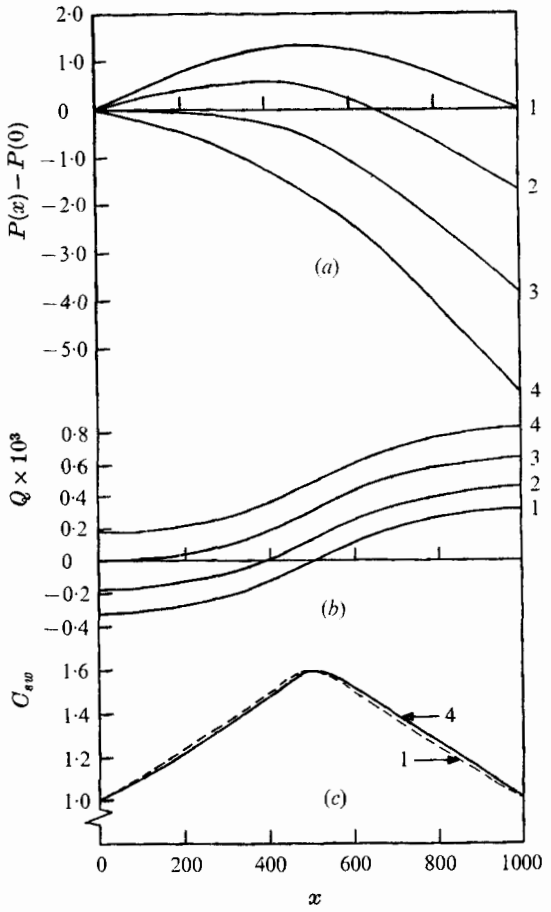

FIGURE 5. Effect of pressure filtration on the distributions of (*a*) pressure, (*b*) volume flux and (*c*) solute concentration in an open-geometry channel with secretory site located in $450 < x < 550$. $\epsilon = 0{\cdot}872 \times 10^{-2}$, $\eta = 0{\cdot}269 \times 10^{-6}$, $R = 0{\cdot}116 \times 10^{-3}$, $C_{sw}(0) = C_{sw}(1000) = 1{\cdot}0$.

(2.25). There is a critical applied pressure differential, see curve 3 of figure 5(*a*), when the filtration pressure is just sufficient to move the stagnation plane to the left-hand end of the channel and thereby balance the water flux due to the local osmosis. A further increase in the applied pressure differential (curve 4 in figures 5(*a*) and (*b*)) results in unidirectional flow along the entire channel.

Figure 5(*c*) shows the nonlinear effect of convection on the streamwise concentration distribution produced by increasing the filtration pressure ΔP across the channel. Non-dimensional filtration pressures of $O(1)$ are typical of epithelial cell layers such as the ciliary body. The total passive water movement due to the local osmosis produced by the active transport is directly proportional to the total area under the concentration curve. We therefore conclude from figure 5(*c*) that the concentration distribution is not significantly altered by convection and hence that the driving forces due to active transport and pressure filtration are essentially independent for epithelial cell layers. Thus the channel efflux $Q(L)$ is linearly related to ΔP and η, the dimensionless secretory site strength. This

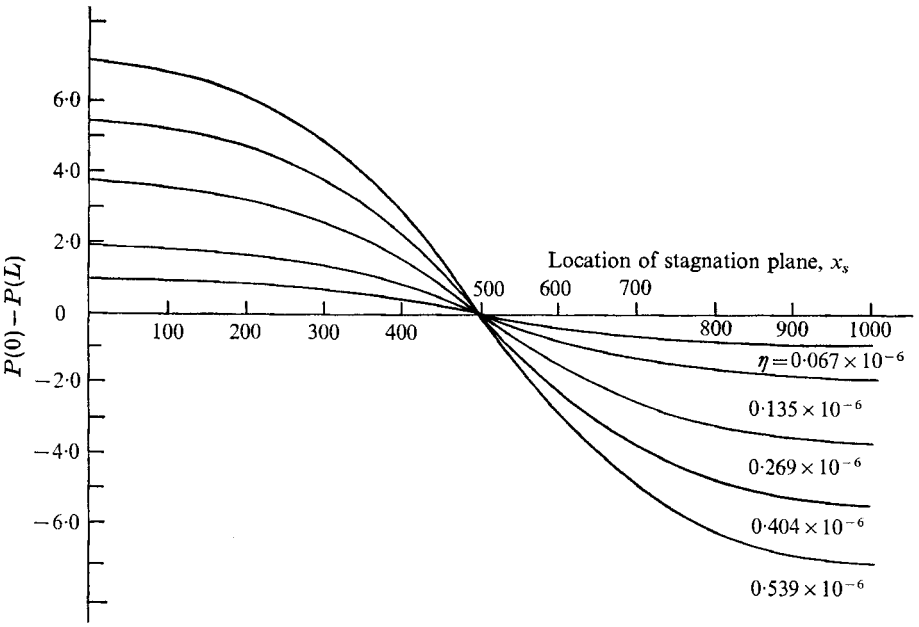

FIGURE 6. Effect of ΔP and η on the shift of stagnation plane in an open-geometry channel with secretory site located in $450 < x < 550$. $\epsilon = 0{\cdot}872 \times 10^{-2}$, $\eta = 0{\cdot}269 \times 10^{-6}$, $R = 0{\cdot}116 \times 10^{-3}$, $C_{sw}(0) = C_{sw}(1000) = 1{\cdot}0$.

linear relation between membrane fluxes and driving forces is the fundamental simplifying hypothesis used in the irreversible thermodynamics theory of membrane transport and is also the basis for the perturbation expansions (3.6) used here. $C_1^{(1)}$ and $C_2^{(1)}$ in (3.6) can be viewed as the lowest order convective corrections to the linear theory.

Figure 6 shows the effect of varying the secretory site strength (value of η) on the movement of the stagnation plane for a symmetric channel. The $\eta = 0{\cdot}269 \times 10^{-6}$ curve is obtained from the intersections with $Q = 0$ axis of the curves in figure 5(*b*). Increasing the secretory site strength is equivalent to increasing the local osmotic effect and thus results in a smaller stagnation plane shift for constant ΔP. The interesting feature of these curves is that the movement of the stagnation plane is a highly nonlinear function of ΔP although, as just noted, epithelial membranes function in a region where all fluxes and driving forces are linearly related. The local value of $Q(x)$ is linearly related to ΔP, but unlike the flux at the channel exit $Q(L)$, it is a nonlinear function of position since the local integrated area under the concentration curve, and hence the local integrated passive water movement due to local osmosis, varies nonlinearly with position. The location of the stagnation plane is determined by the balance between the filtration flux and the integrated passive water movement due to local osmosis between the active transport site and the stagnation plane. On the other hand, the critical value of ΔP required to shift the stagnation plane to the channel entrance, the intersection of the curves in figure 6 with the ΔP axis, is almost linearly proportional to η. This is a result of the fact that the total

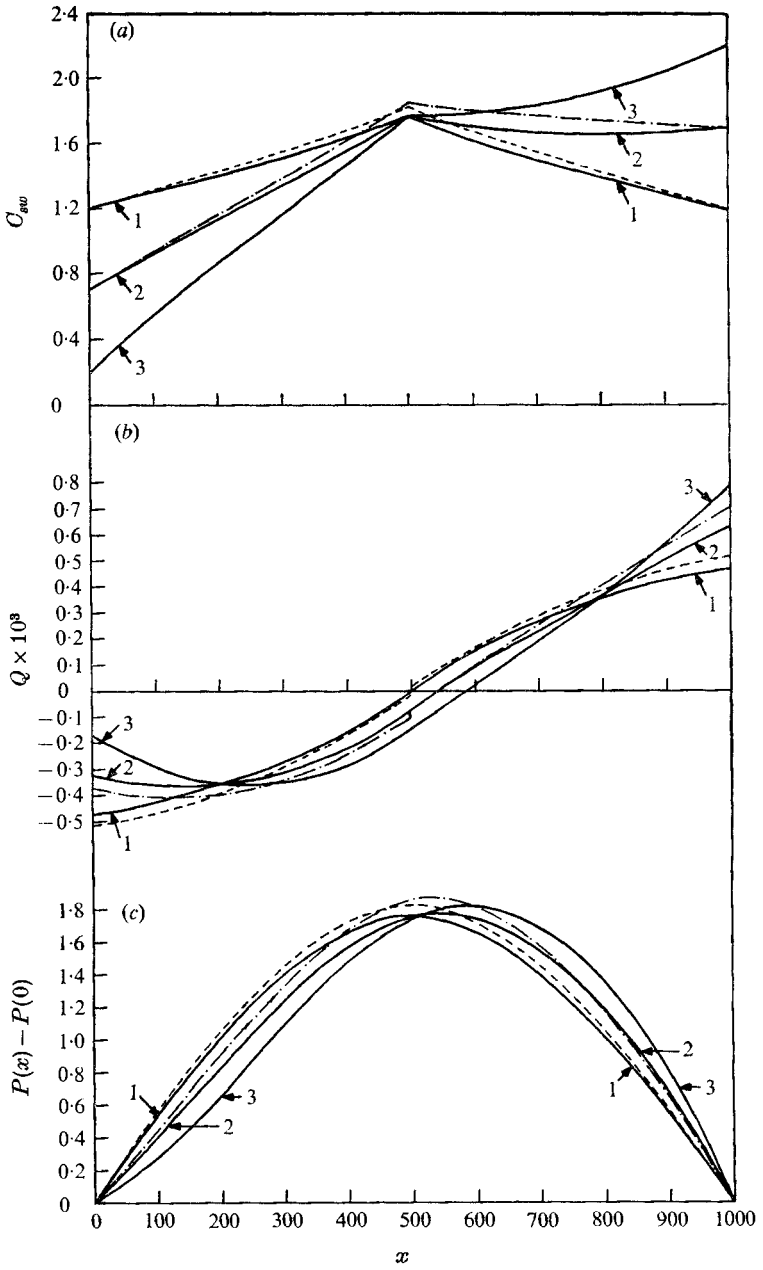

FIGURE 7. Effect of ΔC_{sw} on the distributions of (*a*) solute concentration, (*b*) volume flux and (*c*) pressure in an open-geometry channel with secretory site located in $490 < x < 510$. $\Delta C = 0$, 1·0 and 2·0 for curves 1, 2 and 3 respectively. Comparison with approximate analytical solution for point-source secretory site: – – –, $\Delta C = 0$; –·–·–, $\Delta C = 1$. $\epsilon = 0{\cdot}872 \times 10^{-2}$, $\eta = 1{\cdot}345 \times 10^{-6}$, $R = 0{\cdot}116 \times 10^{-3}$.

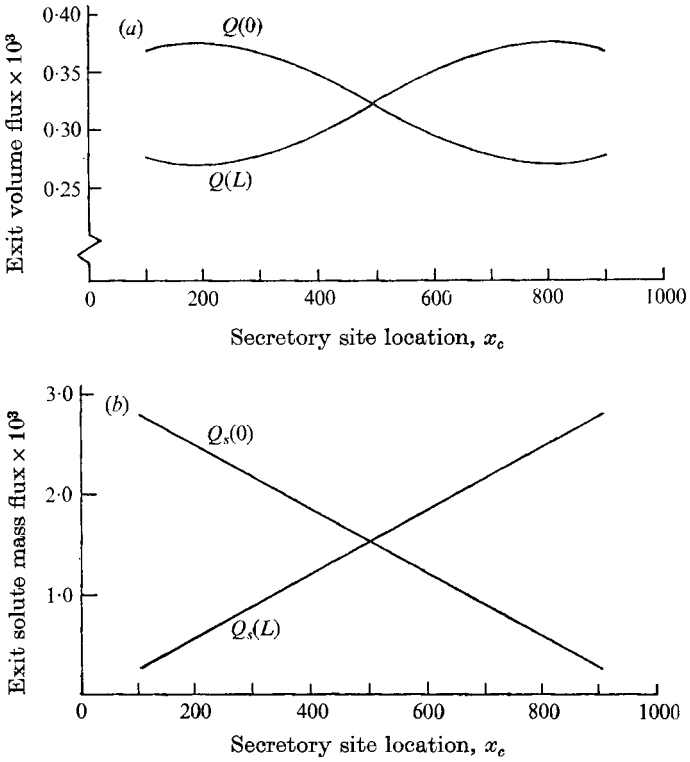

FIGURE 8. Effect of location of the centre of the secretory site on (*a*) the volume fluxes and (*b*) the mass fluxes at the end stations of an open-geometry channel with $\Delta P = \Delta C_{sw} = 0$, secretory site length = 100, $\epsilon = 0{\cdot}872 \times 10^{-2}$, $\eta = 0{\cdot}269 \times 10^{-6}$, $R = 0{\cdot}116 \times 10^{-3}$.

area under the concentration curve, and hence the total local osmotic flux, is independent of ΔP if the nonlinear effects of convection can be neglected.

Figures 7(*a*), (*b*) and (*c*) show the effect of applying an osmotic driving force ΔC_{sw} across a membrane with active transport, but no transmembrane pressure differential. The total passive water movement is the same for each set of curves and again the secretory site is located symmetrically between the end stations. These curves provide a convenient test of the accuracy of the approximate analytical solutions presented in § 3. For the numerical solutions the secretory site had a finite length equal to two per cent of the channel length whereas in the analytic solutions it is treated as a point source. The discontinuity in Q at the secretory site for the analytic curves is due to the active transport of salt and is the ϵS term in the matching condition (3.5*c*). The concentration curves in figure 7(*a*) show the nearly linear diffusion dominated behaviour predicted by the lowest order analytic solutions (3.14*c*) and (3.14*d*). The analytic volume flux curves in figure 7(*b*) are the solutions (3.15*a*) and (3.15*b*), in which the relationship between x and the strained co-ordinate x_0 is obtained from (3.7), (3.17*a*) and (3.17*b*). The curves in figure 7(*c*) show the effect of an osmotic driving force on the pressure distribution in the channel with ΔP maintained at zero. The osmotic driving force has basically redistributed the fluxes $Q(0)$ and $Q(L)$

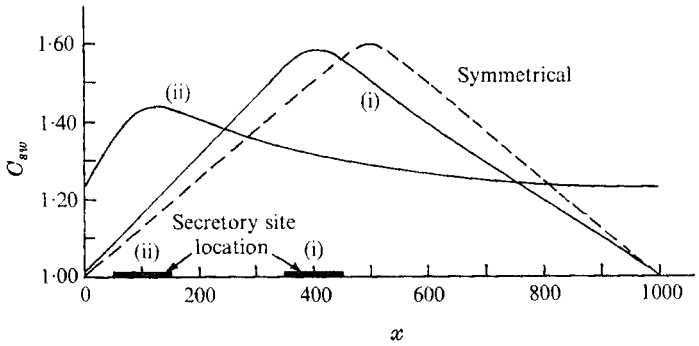

FIGURE 9. Effect of secretory site location on the solute concentration distribution in an open-geometry channel with $\Delta P = \Delta C_{sw} = 0$ and constant passive water flux.

$$\epsilon = 0{\cdot}872 \times 10^{-2}, \quad \eta = 0{\cdot}269 \times 10^{-6}, \quad R = 0{\cdot}116 \times 10^{-3}.$$

to the two end stations, while their sum is a constant since the total passive water movement is held fixed.

In figures 8(*a*) and (*b*) and 9 we examine the effect of secretory site location on the water and solute fluxes at the channel entrance and exit and on the concentration distribution in the channel. The only driving force is active transport. The total passive water movement into the channel is again held constant. Thus the area under each of the curves in figure 9 is the same. The interesting feature is that distribution of the solute fluxes to the two end stations is a much more sensitive function of secretory site location than that for the water fluxes. The salt fluxes at the channel entrance and exit depend principally on the diffusional gradient at the end stations established by the concentration profile and, therefore, vary significantly with secretory site location, see figure 9 or equations (3.14*c*, *d*). On the other hand, the distribution of the water flux at the channel ends is primarily controlled by the filtration pressure differential and not the concentration distribution. One recalls from figure 7(*c*) that changes of $O(1)$ in the concentration profile produced relatively small changes in the pressure distribution provided $\Delta P = 0$.

Figures 5–9 are based on hypothetical open channel geometries and boundary conditions in which we have examined separately the effects of the various driving forces and the secretory site location on the water and solute flux distributions within the channel. In figures 10(*a*) and (*b*) these various elements have been combined in an attempt to model quantitatively a real membrane, the rabbit ciliary body epithelium. This membrane has been selected since there exists a detailed set of experimental measurements (Cole 1961, 1962) which can be used to assess the validity of the theoretical model. These include measurements of the exit volume and solute fluxes and the active transport component of the solute flux for rabbit ciliary body epithelia both *in vivo* and when excised. The values predicted theoretically for these fluxes could be extrapolated to a reasonable accuracy from the results for a single channel using the measured total area of the membrane and an estimate of the average cell and channel dimensions. These dimensions were obtained from observation of high resolution

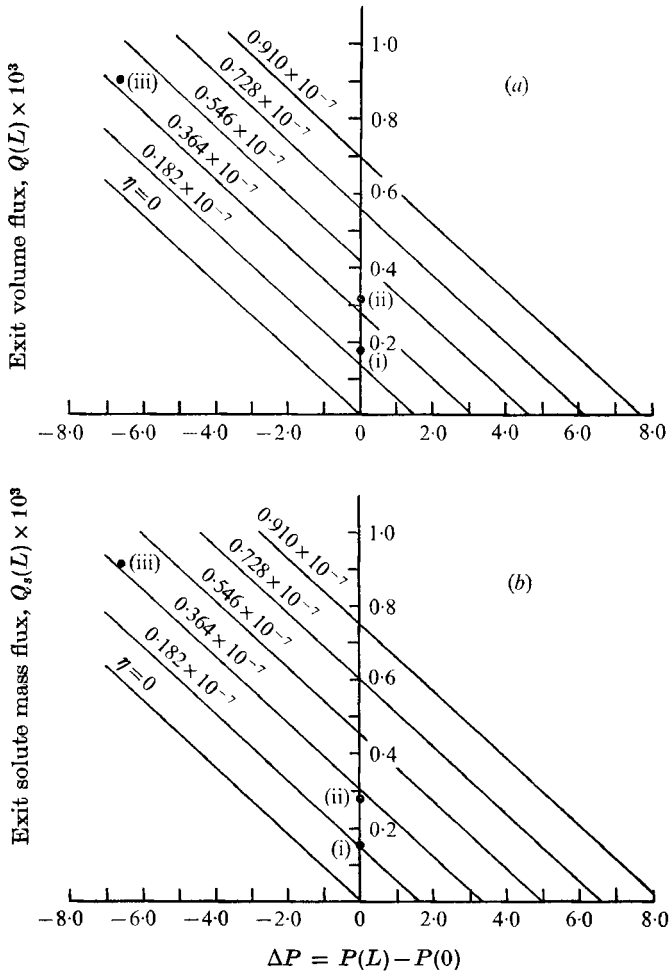

FIGURE 10. Effect of ΔP and η on (*a*) the exit volume flux and (*b*) the exit mass flux in an open-geometry channel with the secretory site located in $690 < x < 790$. $L = 925$, $\epsilon = 0{\cdot}872 \times 10^{-2}$, $R = 0{\cdot}0156$. Point (i) indicates Cole's *in vitro* experimental data, point (ii) an estimate of *in vivo* flux with no filtration and point (iii) Cole's *in vivo* experimental data.

electronmicrographs; these same observations gave an average dimensionless channel length $L = 925$.

For excised preparations Cole found that the exit volume and solute fluxes were equivalent, respectively, to $Q(L) = 0{\cdot}173 \times 10^{-3}$ and $Q_s(L) = 0{\cdot}155 \times 10^{-3}$. The latter value was based on the measured short-circuit current, that is the equivalent electron current measured when a low resistance shunt is placed across the membrane and the transmembrane potential difference reduced to zero. These data points are labelled (i) in figures 10(*a*) and (*b*) and, since $\Delta P = 0$, lie on the vertical axis. The *in vivo* value of ΔP is the pressure difference between the intraocular pressure and the blood diastolic pressure in the capillary bed. For the eye *in vivo* Cole obtained values equivalent to

$$Q(L) = 0{\cdot}9 \times 10^{-3}, \quad Q_s(L) = 0{\cdot}91 \times 10^{-3},$$

and from the short-circuit current an active transport component of

$$Q_s(L) = 0{\cdot}28 \times 10^{-3}.$$

It is to be noted that both the volume and solute fluxes measured *in vivo* were more than five times greater than those in the excised preparation, while the active transport component increased by less than a factor of 2. This intriguing behaviour is one of the fundamental unanswered questions in ciliary body transport.

The curves in figures 10(*a*) and (*b*) represent the theoretical solutions for the exit volume and solute fluxes in a channel with active transport and pressure filtration but isotonic end stations. The secretory site was centred at $x = 740$, which places it at the beginning of the apical infoldings of the non-pigmented cell layer, see figure 2; this is the location suggested by histochemical studies of Na + K-ion-dependent ATPase activity. The ion pump strength η is treated as a fixed parameter and is determined by the experimentally measured short-circuit current. The appropriate η curve corresponding to Cole's *in vitro* ($\Delta P = 0$) experiments with the excised eye is shown as point (i) in figure 10(*b*). This value of η is $0{\cdot}182 \times 10^{-7}$; ϵ is measured similarly. Only the parameter R of the three dimensionless groups η, ϵ and R is not accurately known. To circumvent this difficulty R was chosen by curve fitting one of the three experimental points in figure 10(*a*) for the volume flux, namely point (iii). Thus, two of the six experimental points in figures 10(*a*) and (*b*) are used to determine the free parameters in the governing equations, while the remaining four points are a true test of the theoretical model. To obtain the theoretically predicted volume flux the intersection of the $\eta = 0{\cdot}182 \times 10^{-8}$ curve with the $\Delta P = 0$ axis is located in figure 10(*a*). The predicted value $Q(L) = 0{\cdot}142 \times 10^{-3}$ is within 20% of the measured volume flux $Q(L) = 0{\cdot}173 \times 10^{-3}$. In view of the uncertainty in the dimensionless group R, the neglect of electrical effects and other model refinements this agreement between theory and experiment is satisfactory.

The *in vivo* results cannot be compared directly with the *in vitro* data but must first be corrected for the increased active transport that results from the increased metabolism. It is evident, however, from the curves in figure 10 that for the prescribed values of η, ϵ and R the fluxes and driving forces are linearly related. Thus, the active transport component of the total volume flux in the living eye, $Q(L)$ when $\Delta P = 0$, can be determined by assuming a linear relation between the *in vitro* and *in vivo* short-circuit current measurements and the corresponding *in vitro* volume flux. $Q(L)$ with $\Delta P = 0$ for the eye *in vivo* is shown as point (ii) in figure 10(*a*) and has the value $0{\cdot}313 \times 10^{-3}$. The new value of η corresponding to the increased active transport rate is, therefore, about $0{\cdot}4 \times 10^{-7}$. Since η remains constant, the experimentally measured volume flux $Q(L) = 0{\cdot}9 \times 10^{-3}$, point (iii) in figure 10(*a*), is achieved for a dimensionless interstitial–intraocular pressure differential $\Delta P = -6{\cdot}6$, the minus sign appearing because of the direction in which the pressure difference is measured. In dimensional units this ΔP is equivalent to 80 mm Hg, which when corrected for the small osmolarity differences between blood plasma and aqueous humour gives an equivalent ΔP of approximately 50–60 mm Hg. Returning to figure 10(*b*) we

note that the theoretical predictions for the exit solute flux for $\eta = 0{\cdot}4 \times 10^{-3}$ are $Q_s(L) = 0{\cdot}94 \times 10^{-3}$ for $\Delta P = -6{\cdot}6$ and that $Q_s(L) = 0{\cdot}33 \times 10^{-8}$ when $\Delta P = 0$, corresponding to the theoretically predicted active transport component. The corresponding experimentally measured values, points (iii) and (ii) respectively, are $Q(L) = 0{\cdot}91 \times 10^{-3}$ and $Q_s(L) = 0{\cdot}28 \times 10^{-3}$, the latter being based on the short-circuit current measurement. Both values are obviously in as close an agreement with the theory as one is justified to expect considering the sophistication of the quantitative model.

In summary, the theoretical model predicts that the marked increase in fluid transport in the living rabbit eye compared with that in the dead rabbit eye is due to the hydrostatic pressure difference between the blood and the aqueous humour. These results when combined with the earlier experiments of Davson (1953), which showed that *p.* amino hippinate M.W. 194 and raffinose M.W. 594 could pass with equal facility through the ciliary body epithelium, and Langham's (1958, 1959) intraocular pressure experiments with cat's eyes provide cogent evidence that the extracellular channels in the ciliary process are open and provide the transport route for the observed water and solute movement. In contrast to previous qualitative models, which attributed the bulk water movement solely to active transport, the present quantitative model shows that the formation of aqueous humour is a pressure-dependent mechanism and that the ion pumps are responsible for only about one-third of the total water movement. Results not shown indicate that this active transport fraction is even less for cat's eyes, where it accounts for about one-tenth of the total flux.

6. Partial occlusions

The results of §§ 3, 4 and 5 have been confined to constant-height extracellular channels. However, as noted in § 1, electron micrographs of the ciliary body epithelium clearly indicate localized regions in which the channel is partially occluded. In this section we shall briefly consider the effect of such constrictions on the streamwise pressure and concentration distribution within the channel. To simplify the analysis we shall assume that there is no active solute transport in the obstructed region and that on the length scale l of the obstruction the passive movement of water across the lateral boundaries can be neglected. We shall assume in addition that the inertial forces within the occlusion are small compared with the viscous forces, that the normal component of the momentum equation can be neglected and that the concentration varies only as a function of x, the instantaneous mixing hypothesis invoked in § 3.

Introducing the simplifications outlined in the last paragraph, impermeable lateral boundaries and a uniform concentration profile, equations (2.22) and (2.23) become

$$\frac{2}{3}\frac{d}{dx}(U_m h) = 0, \tag{6.1}$$

$$\frac{2}{3}\frac{d}{dx}(U_m h C_s) - \frac{d}{dx}\left(h\frac{dC_s}{dx}\right) = 0. \tag{6.2}$$

Substituting (6.1) into (6.2) and using (2.26a) gives

$$\frac{d^2C_s}{dx^2}-\frac{1}{h}\left(Q-\frac{dh}{dx}\right)\frac{dC_s}{dx}=0. \tag{6.3}$$

One integration of this equation gives

$$\frac{dC_s}{dx}=\frac{S(0)\,h(0)}{h}\exp\left(Q\int_0^x\frac{dx}{h}\right), \tag{6.4}$$

where $x=0$ here refers to the beginning of the occlusion, $S(0)=dC_s(0)/dx$ is the initial concentration gradient and Q is a constant in view of (2.26) and (6.1). A second integration yields the final result:

$$C_s(x)-C_s(0)=\frac{S(0)\,h(0)}{Q}\left\{\exp\left(Q\int_0^x\frac{dx}{h}\right)-1\right\}. \tag{6.5}$$

The streamwise variation in pressure is obtained from an integration of (2.25), which gives

$$P(x)-P(0)=-12Q\int_0^x\frac{dx}{h^3}. \tag{6.6}$$

Solutions (6.5) and (6.6) are particularly useful in that they apply to an arbitrarily varying channel height $h(x)$. Equation (6.6) is a well-known result in lubrication theory.

One convenient form for $h(x)$, which is representative of a typical occlusion geometry, is the sinusoidal variation

$$h(x)/h(0)=1-\tfrac{1}{2}(1-h_t/h(0))\,(1-\cos 2\pi x/l), \tag{6.7}$$

which is sketched in the upper left-hand corner of figure 11. Equation (6.7) describes a one-parameter family of constriction geometries which depend only on the ratio of throat to initial area $h_t/h(0)$.

Substituting (6.7) into (6.5) and integrating across the constriction yields

$$C_s(l)-C_s(0)=\frac{S(0)\,h(0)}{Q}\left\{\exp\left[\frac{Ql}{h(0)}\left(\frac{h(0)}{h_t}\right)^{\frac{1}{2}}\right]-1\right\}. \tag{6.8}$$

If (6.8) is now divided by the concentration differential across a uniform section of channel with the same length, initial height and concentration gradient, we have

$$\frac{\Delta C_c}{\Delta C_u}=\frac{\exp\left(QlK/h(0)\right)-1}{\exp\left(Ql/h(0)\right)-1}, \tag{6.9}$$

where $K=h(0)/h_t$, and ΔC_c and ΔC_u represent the concentration differentials for a constricted and unconstricted channel respectively. Similarly substitution of (6.7) in (6.6) gives

$$P(l)-P(0)=\Delta P_c=\tfrac{3}{2}(Ql/h(0)^3)\,(3K^5+2K^3+3K).$$

If this result is now divided by the Poiseuille pressure drop ΔP_u across a constant-area channel with the same volume flux Q, length l and initial height $h(0)$ we obtain

$$\Delta P_c/\Delta P_u=\tfrac{3}{8}K^5+\tfrac{1}{4}K^3+\tfrac{3}{8}K. \tag{6.10}$$

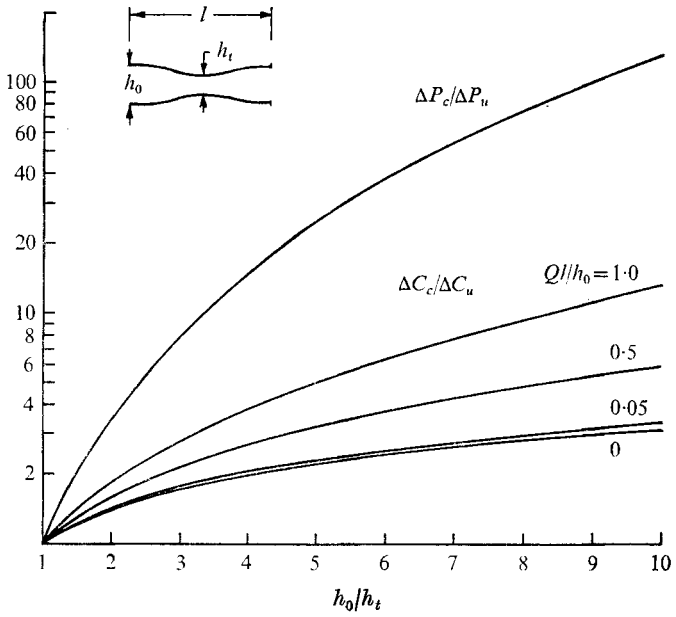

FIGURE 11. Effect of a partial occlusion on the streamwise pressure and concentration gradient across an open-geometry channel.

The solution for $\Delta C_c/\Delta C_u$ depends on two dimensionless groups, $Ql/h(0)$ and K, whereas $\Delta P_c/\Delta P_u$ depends only on K. This is not surprising since the convective terms are omitted in the momentum equation (2.25) but are retained in the solute conservation equation (6.2). In the limit as this convective contribution vanishes, $Ql/h(0) \to 0$ and $\Delta C_c/\Delta C_u$ in (6.9) becomes a function of K only, as can be observed from figure 11.

Equations (6.9) and (6.10) have been plotted in figure 11. Since the pressure gradient in a uniform channel is constant the ratio $\Delta P_c/\Delta P_u$ can be interpreted as the ratio of the length of a uniform channel required to produce a pressure drop equalling that across the occluded zone to the length of the occluded zone. The constriction also produces an increased concentration differential; however, this effect is much less pronounced than that for the pressure field for the same value of $h(0)/h_t$ provided that $Ql/h(0) \leqslant O(1)$. For constrictions typical of the ciliary body epithelium, we anticipate results very close to the limiting behaviour for $Ql/h(0) = 0$.

Equation (6.8) can also be used to show the importance of convection in a constant-area channel. To derive this condition we set $h(0)/h_t = 1$ in (6.8) and divide by the linear concentration drop $\Delta C_{Q=0} = S(0)\,L$ that would occur in a purely diffusive channel ($Q = 0$) of length L:

$$\Delta C_u/\Delta C_{Q=0} = (h(0)/QL)\{\exp[QL/h(0)] - 1\}. \tag{6.11}$$

For $QL/h(0) \ll 1$ the ratio in (6.11) is given approximately by

$$\Delta C_u/\Delta C_{Q=0} = 1 + \tfrac{1}{2}(QL/h(0)). \tag{6.12}$$

The deviation from the purely diffusive solution as predicted by (6.11) or (6.12) is underestimated since the passive water movement at the lateral boundaries is neglected. These results clearly show that even if $Q \ll 1$ convective effects will eventually become important if the channel is sufficiently long for $QL/h(0)$ to be $\geqslant O(1)$. This, of course, is the motivation behind the use of the co-ordinate straining technique employed in § 3.

The authors wish to express their appreciation to Dr Robert Graff of the City College of the City University of New York, Dr Maurice Langham and Dr Keith Green of the Wilmer Institute, Johns Hopkins University School of Medicine for their many helpful discussions and insights. The first author was partially supported in this work by a grant from the Research Foundation of the City University of New York. The second author was supported by a National Science Foundation, Science Faculty Fellowship for the year 1969–70 while a doctoral student in the Department of Mechanical Engineering of the City College. A preliminary version of this paper was presented at the A.I.A.A. 9th Aerospace Sciences Meeting 1971, New York (see *A.I.A.A. Paper*, no. 71–105).

REFERENCES

Cole, D. F. 1961 *Br. J. Ophthalmal.* **45**, 202.
Cole, D. F. 1962 *Br. J. Ophthalmal.* **46**, 577.
Davson, H. 1953 *J. Physiol.* **122**, 10*P*.
Diamond, J. M. 1964 *J. Gen. Physiol.* **48**, 15.
Diamond, J. M. & Bossert, W. H. 1967 *J. Gen. Physiol.* **50**, 2061.
Diamond, J. M. & Tormey, J. M. 1966 *Nature*, **210**, 817.
Goldgraben, J. R. 1972 Ph.D. thesis, City University of New York.
Langham, M. E. 1958 *Physiol. Rev.* **38**, 215.
Langham, M. E. 1959 *J. Physiol.* **147**, 29.
Segel, L. A. 1970 *J. Theor. Biol.* **29**, 233.